Site-Specific Characterization of HIV-1 Nucleocapsid Protein Binding to Oligonucleotides with Two Binding Sites[†]

Sergiy V. Avilov,[‡,§] Julien Godet,[‡] Etienne Piémont,[‡] and Yves Mély*[,‡]

Laboratoire Biophotonique et Pharmacologie, UMR 7213 CNRS, Université de Strasbourg, Faculté de Pharmacie, 74 route du Rhin, 67401 Illkirch, France, and Palladin Institute of Biochemistry, 9, Leontovich street, 01030 Kiev, Ukraine

Received December 8, 2008; Revised Manuscript Received January 30, 2009

ABSTRACT: The nucleocapsid protein (NC) of HIV-1 is a highly conserved protein essential for the virus life cycle that constitutes an attractive target for new antiviral agents. Most NC functions rely on its binding to the HIV-1 genomic RNA and its DNA copies that contain multiple and possibly interdependent binding sites. Therefore, a detailed understanding of NC binding requires a site-specific experimental approach. We have recently shown that 2-aminopurine (2Ap), a fluorescent adenine analogue, can site-selectively probe the binding of NC. Here, we introduced 2Ap at various positions of model single-stranded dodecanucleotides containing two TG motifs which constitute putative specific binding sites. Steady-state and time-resolved fluorescence experiments indicated that NC binding strongly increased the fluorescence quantum yield of 2AP by reducing the dynamic quenching of 2Ap by its close neighbors and slowing the picosecond to nanosecond conformational fluctuations of the oligonucleotides. The dodecanucleotides were found to bind two NC molecules at physiological salt concentrations, confirming the preferential binding of NC to TG motifs and an occluded binding site size for NC of five to six bases. Using the NC-induced changes in 2Ap fluorescence, we determined the microscopic affinity constants of the individual binding sites and showed that affinities can significantly differ from one site to another within the same dodecanucleotide, depending on the position of the TG dinucleotide and the nature of its close neighbors. Moreover, our data suggest that binding of NC even to close binding sites shows no strong cooperativity.

HIV-1 nucleocapsid protein (NC),[1] either as a domain of the Gag polyprotein precursor or as a mature protein, is essential for several important steps of the virus life cycle (*1*). For instance, selection of viral genomic RNA for packaging into virions is mediated by binding of the NC domain within Gag to the ψ encapsidation sequence within the untranslated region of the HIV-1 genome (*2*). Further, NC chaperones the annealing of the primer tRNA to the primer binding site, and the two obligatory strand transfers necessary for the synthesis of a complete proviral DNA by reverse transcriptase (*3*−*5*). Mature NC is a basic protein of 55 amino acids (Figure 1) containing two highly conserved $CX_2CX_4HX_4C$ zinc fingers [residues 15−28 and 36−49, termed F1 and F2, respectively (*6*)] with very high affinity for Zn^{2+} ions (*7*). Binding of Zn^{2+} to the fingers results in a highly constrained folded structure in which the two CCHC motifs of NCp7 are spatially close and weakly interacting

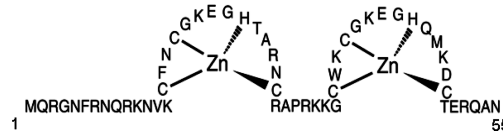

FIGURE 1: Sequence of the HIV-1 nucleocapsid protein.

with one another (*8*−*10*). Mutations of amino acids involved in zinc binding lead to imperfectly folded protein and noninfectious viruses (*11*−*20*). The NC mutant virions contain small amounts of genomic RNA and have defects in reverse transcription. NC is thus an attractive target for the development of new antiviral agents (*1, 21*).

The mechanism of the recognition by NC of its nucleic acid targets is not fully understood. Experiments with NC and short oligonucleotides (ODNs) revealed that at least five bases are needed for stable NC binding (*22*−*24*). Moreover, it was found that NC binds to poly-G better than to any other homopolymer sequence, but much more stable binding was observed for alternating base sequence $(TG)_n$ (*22*). Detailed studies of NC binding to hexanucleotides with systematically varied bases revealed moderate association constants ($\approx 10^5$−10^6 M^{-1}) and a key role of the TG motif for specific binding (*23*). NC binding to its natural targets, namely the stem−loop regions of viral genomic RNA, was studied as well, confirming the preference of NC for TG- or GXG-containing single-stranded sequences (*23, 25*−*27*). NMR structures of several NC−ODN complexes clearly demonstrated that guanine residues play a key role in NC binding,

[†] The study was supported by Agence Nationale de Recherches sur le SIDA (ANRS) and the European consortium 'Targeting Replication and integration of HIV'. S.V.A. was a fellow of Fondation pour la Recherche Medicale, France.

* To whom correspondence should be addressed. Telephone: +33 (0)3 90 24 42 63. Fax: +33 (0)3 90 24 43 12. E-mail: mely@pharma.u-strasbg.fr.

[‡] UMR 7213 CNRS.

[§] Palladin Institute of Biochemistry.

[1] Abbreviations: 2Ap, 2-aminopurine; HIV-1, human immunodeficiency virus type 1; NC, HIV-1 nucleocapsid protein; ODN, oligonucleotide; NMR, nuclear magnetic resonance; PBS, primer binding site; SD, standard deviation.

10.1021/bi8022366 CCC: $40.75
Published on Web 02/02/2009

through stacking with the Trp37 residue of the C-terminal finger motif (*28*−*32*). In fact, Trp37 belongs to a hydrophobic plateau that forms at the top of the folded zinc fingers and is critical for the nucleic acid chaperone properties of NC (*33, 34*). This hydrophobic plateau also includes the Val13, Phe16, Thr24, and Ala25 residues which form additional contacts with the ODN binding sites (*28*−*32*). Moreover, it was found that more than one NC molecule binds to the $(TG)_4$ sequence and more than one octanucleotide can bind to a single NC molecule (*35*). However, the binding constant of the additional ODN is much lower than that in the 1:1 complex. Finally, the parameters for binding of NC to longer DNA and RNA sequences were also reported, but using simplifying assumptions such as single binding sites or identical and independent binding sites (*2, 33, 36*−*40*).

In fact, the analysis of NC binding to ODNs with multiple binding sites is hampered by the intrinsic limitation of most techniques that allow monitoring of the binding in a global manner only, with no ability to discriminate between the different binding sites. Moreover, appropriate models that describe the binding to overlapping binding sites with different affinities and cooperativity are also missing. To circumvent the first limit, ODNs labeled with site-specific reporters can be used. In this respect, we recently demonstrated that 2-aminopurine (2Ap), an environmentally sensitive fluorescent analogue of adenine, may serve as a site-specific sensitive reporter for NC binding (*41*). In the absence of NC, the fluorescence of 2Ap is highly quenched, due to collisions with the neighbor bases that lead to stacking interactions. Binding of NC restricted the ODN flexibility on the picosecond to nanosecond time scale, impeding the collisions of 2Ap with its immediate neighbors, which in turn results in a strong fluorescence increase. As a consequence, 2Ap can probe site-specific conformational and dynamic changes upon NC binding.

In this respect, the aim of this work was to investigate NC binding to three 2Ap-labeled dodecanucleotides that constitute the simplest presumably "multivalent" ODNs. To limit the contributions of multiple overlapping sites in the binding process, all ODNs contained two TG motifs that constitute strong preferential binding sites for NC. The three ODNs differed by the position and proximity of the TG motifs within their sequence and were non-self-complementary and unfolded. To obtain site-specific information, 2Ap was introduced at various positions within these ODNs. We found that the three tested ODNs bound two NC proteins with affinities dependent on the position and on the neighbors of the TG motifs.

MATERIALS AND METHODS

Materials. NC(1−55) (Figure 1) was synthesized on an Applied Biosystems A433 peptide synthesizer as described previously (*42*). Single-stranded DNA dodecanucleotides, unlabeled, covalently labeled with AlexaFluor430 (Invitrogen; further termed "Alexa430"), and 2Ap-substituted, were synthesized and HPLC-purified by IBA. The studied sequences TGACCGTGACCG, AATGACTGAAAC, and AAACTGAATGAC are termed ODN1, ODN2, and ODN3, respectively; 2Ap substitutions are indicated by adding "ApX" to the acronym, where X is the position of the 2-aminopurine residue. All the dodecanucleotides are unfolded at 20 °C according to the mfold software (*43*) (http://frontend.bioinfo.rpi.edu/applications/mfold/). Absorbance spectra were recorded with a Cary 400 UV−vis spectrophotometer (Varian). Concentrations of the ODNs were calculated from their absorbance using the molar extinction coefficients (e_{260}) specified by the supplier. All experiments were performed at 20 °C in 50 mM Hepes (pH 7.5) either with or without 0.1 M NaCl. All chemicals were purchased from Sigma.

Steady-State Fluorescence Spectroscopy. Fluorescence spectra were recorded on a FluoroMax3 spectrofluorimeter (Jobin Yvon) equipped with a thermostated cell compartment. Fluorescence intensities were corrected for buffer fluorescence and screening effects. Quantum yield was calculated using free 2Ap as a reference [0.68 (*44*)], with an excitation wavelength of 315 nm. To determine the constant for binding of NC to the ODNs, fixed concentrations of the 2Ap-containing ODNs were titrated with increasing concentrations of NC, in the presence of 0.1 M NaCl. Excitation and emission wavelengths were 315 and 370 nm, respectively. The parameters were recovered from nonlinear fits of eqs 4a and 5 (see Results) to the experimental data with Microcal Origin 7.0.

Time-resolved fluorescence measurements were performed with the time-correlated, single-photon counting technique, as described previously (*41, 45*). Excitation at 315 and 430 nm for 2Ap and Alexa430 was provided by a pulse-picked frequency-tripled and -doubled Ti-sapphire laser (Tsunami, Spectra Physics), respectively, pumped by a Millenia X laser (Spectra Physics). Emission was collected through a polarizer set at magic angle and an 8 nm band-pass monochromator (Jobin-Yvon H10) set at 370 and 540 nm for 2Ap and Alexa430, respectively. The single-photon events were detected with a microchannel plate Hamamatsu R3809U photomultiplier coupled to a Philips 6954 pulse preamplifier and recorded on a multichannel analyzer (Ortec 7100), calibrated at 25.5 ps/channel. The instrumental response function was recorded with a polished aluminum reflector, and its full width at half-maximum was 40 ps. Fluorescence intensity decays [$I(t)$] were analyzed as a sum of exponentials: $I(t) = \sum\alpha_i \exp(-t/\tau_i)$, where τ_i values are the fluorescence lifetimes and α_i values are the associated amplitudes such that $\sum\alpha_i = 1$. The mean lifetime was calculated according to the relationship $\langle\tau\rangle = \sum\alpha_i\tau_i$. The population, α_0, of 2Ap dark species within the ODNs was calculated with the relationship $\alpha_0 = 1 - \tau_{free}/(\tau_{sample}R_m)$, where τ_{free} is the lifetime of free 2Ap, τ_{sample} is the measured lifetime of 2Ap within a given ODN (either free or bound to NC), and R_m is the ratio of the corresponding steady-state fluorescence intensities. The remaining amplitudes, α_{ic}, were recalculated from the measured amplitudes, α_i, according to the relationship $\alpha_{ic} = \alpha_i(1 - \alpha_0)$.

For time-resolved anisotropy measurements, the fluorescence decay curves were recorded at vertical and horizontal positions of the polarizer, as described previously (*41*). Time-resolved fluorescence anisotropy decays were analyzed with the following equations:

$$I_{\parallel}(t) = I(t)[1 + 2r(t)]/3$$

$$I_{\perp}(t) = I(t)[1 + r(t)]/3$$

$$r(t) = \frac{I_{||}(t) - GI_{\perp}(t)}{I_{||}(t) + 2GI_{\perp}(t)} = r_0 \sum \beta_i \exp(-t/\varphi_i) \qquad (1)$$

where β_i values are the amplitudes of the rotational correlation times φ_i, $I_{||}$ and $I_{\perp}$ are the intensities collected at emission polarizations parallel and perpendicular, respectively, to the polarization axis of the excitation beam, and G is the geometry factor at the emission wavelength, determined in independent experiments. The fundamental anisotropy r_0 value (0.33) was determined independently for 2Ap in 77% glycerol (v/v) (*41*) and was fixed in the analysis of the time-resolved anisotropy data. The theoretical values of the rotational correlation times for the ODNs and their complexes were calculated assuming spherical shapes, by

$$\phi = \frac{\eta M(\upsilon + h)}{RT} \qquad (2)$$

where η is the viscosity, T is the temperature, υ is the specific volume of the particle, h is the degree of hydration, and R is the molar gas constant. Values of 0.78 and 0.4 mL/g were taken for the specific volume and the degree of hydration, respectively.

Time-resolved intensity and anisotropy data were treated with a nonlinear least-squares analysis using a homemade program (kindly provided by G. Krishnamoorthy). In all cases, the χ^2 values were close to 1, and the weighted residuals were distributed randomly around zero, indicating an optimal fit.

RESULTS

Characterization of the Dodecanucleotides and Their Complexes with NC by 2Ap Fluorescence. 2Ap was introduced into various positions within three single-stranded DNA dodecanucleotide sequences (ODN1, ODN2, and ODN3) containing two TG motifs at different positions (Table 1). We observed that the fluorescence spectra of the 2Ap-labeled dodecanucleotides, like free 2Ap and hexanucleotides, exhibit an emission maximum around 370 nm (not shown). The quantum yield of 2Ap in these ODNs was quite low (Table 1), indicating a strong quenching of 2Ap fluorescence by the neighbor bases (for a review, see ref *46*). Quenching is the strongest (quantum yields in the range of 0.007−0.019) when 2Ap is flanked by a guanine (ODN1Ap3, ODN1Ap9, ODN2Ap5, ODN3Ap7, and ODN3Ap11), consistent with the fact that G is the most efficient quencher of 2Ap among the natural bases (*47*). The remaining sequences (ODN2Ap2, ODN2Ap10, and ODN3Ap3) exhibit nearly identical quantum yields (0.045−0051), though the nature of the 3′-flanking residue of 2Ap differs in these three sequences. This indicated that the nature of this residue does not markedly influence the 2Ap quantum yield. The time-resolved intensity decays of the dodecanucleotides (Table 1 of the Supporting Information) showed multiple lifetimes, attributed to picosecond to nanosecond conformational fluctuations of the 2Ap-labeled ODNs in the excited state that drive 2Ap from unstacked to stacked conformations.

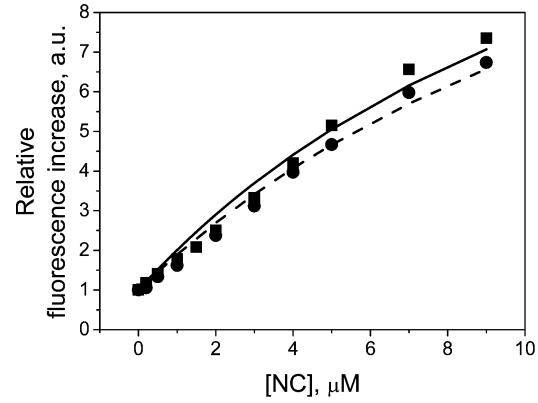

FIGURE 2: Influence of 2Ap substitution on the binding to NC. The 2Ap-labeled ODN2Ap5 sequence was titrated with NC either in the absence (■, solid line) or in the presence of an equimolar concentration of the corresponding nonlabeled ODN (●, dashed line). The total ODN concentration was 2 μM in both cases.

Probing NC−dodecanucleotide interactions by 2Ap is only valid if the substitution of a natural base by 2Ap does not affect the interaction. We have shown previously that 2Ap substitution does not significantly influence NC binding to AATGCC and AACGCC sequences (*41*). To demonstrate that 2Ap substitution does not also affect NC binding to the studied dodecanucleotides, the titration curves of 2 μM 2Ap-labeled dodecanucleotides with NC were compared to the titration curves obtained using an equimolar mixture of labeled and nonlabeled sequences at the same concentration. The data with ODN1Ap3, taken as a representative example, are illustrated in Figure 2. The binding curves were found to be very similar, indicating that 2Ap-labeled and native sequences exhibit comparable affinities. Thus, substitution of A with 2Ap does not significantly influence NC binding. Similar results were obtained for all substituted positions (data not shown).

When NC binds, the fluorescence quantum yield of 2Ap within the dodecanucleotides significantly increases (Table 1), but the position of the emission maximum does not change (data not shown), indicating that NC binding

Table 1: Quantum Yields and NC Binding Constants of the 2Ap-Substituted Dodecanucleotides

	sequence	quantum yield, free ODN[a]	quantum yield, ODN + NC[a]	k_1 ($\times 10^{-6}$ M^{-1})[b]	k_2 ($\times 10^{-6}$ M^{-1})[b]
ODN1Ap3	TGApCCGTGACCG	0.007	0.078	0.41	
ODN1Ap9	TGACCGTGApCCG	0.009	0.135		1.40
ODN2Ap2	AApTGACTGAAAC	0.046	0.202	0.87	
ODN2Ap5	AATGApCTGAAAC	0.012	0.194	0.81	
ODN2Ap10	AATGACTGAApAC	0.051	0.105		1.80
ODN3Ap3	AAApCTGAATGAC	0.045	0.173	0.66	
ODN3Ap7	AAACTGApATGAC	0.015	0.198	0.70	0.30
ODN3Ap11	AAACTGAATGApC	0.019	0.167		0.44

[a] Quantum yields were calculated assuming a quantum yield of 0.68 for free 2Ap (*44*). The standard error of the mean was less than 15%, for at least three measurements. [b] The microscopic ("site-specific") equilibrium binding constants were obtained by fitting the data of Figure 3 to eqs 4a and 4b, with the exception of the ODN3Ap7 data which were fitted to eq 5. The standard error of the mean for three measurements was less than 20%. Excitation was at 315 nm. Emission was at 370 nm and was corrected for inner-filter effects and buffer fluorescence.

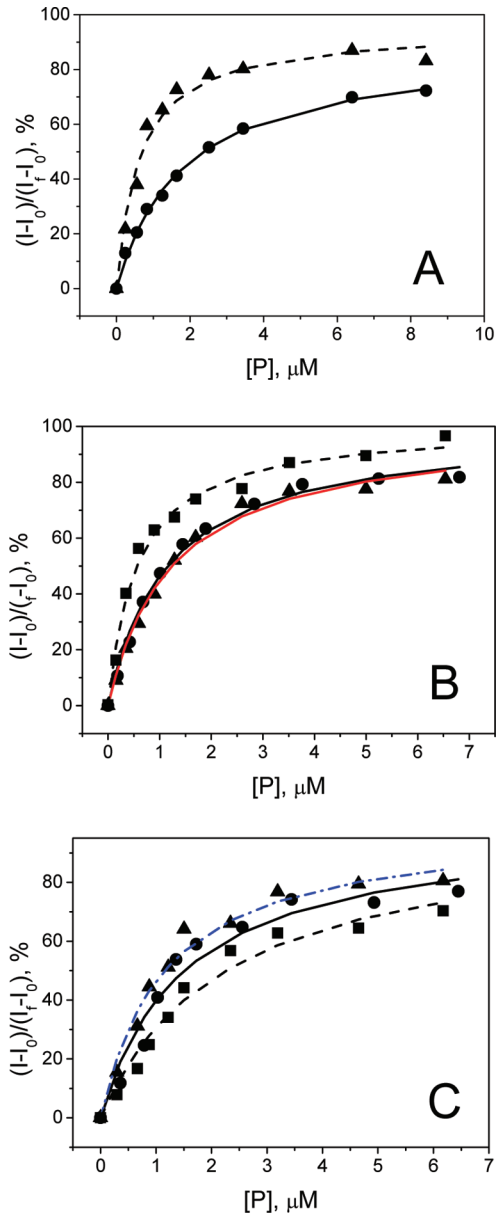

FIGURE 3: Titration curves of 2Ap-substituted dodecanucleotides with NC. The relative 2Ap fluorescence intensity changes $(I - I_0)/(I_f - I_0)$ were plotted as a function of the free NC concentration calculated with eq 3. Excitation was at 315 nm and emission at 370 nm. The ODN concentration was 2 μM in 50 mM Hepes (pH 7.5) and 0.1 M NaCl. Titrations were performed with (A) ODN1 labeled by 2Ap at position 3 (●, solid line) or 9 (▲, dashed line), (B) ODN2 labeled by 2Ap at position 2 (●, black solid line), 5 (▲, red solid line), or 10 (■, dashed line), and (C) ODN3 labeled at position 3 (●, solid line), 7 (▲, blue dashed−dotted line), or 11 (■, dashed line). The solid and dotted lines correspond to the fits of the experimental points with eqs 4a and 4b, respectively. The blue dashed−dotted line in Figure 3C corresponds to the fit of ODN3Ap7 with eq 5.

significantly reduces the level of quenching of 2Ap fluorescence by its neighbor bases but does not change the polarity of its surroundings. The NC-induced increase in the fluorescence quantum yield was found to depend on the 2Ap position and the ODN sequence, ranging from 2.1-fold for ODN2Ap10 to 16-fold for ODN2Ap5. The strongest fluorescence increase was observed when 2Ap is next to a G residue. Interestingly, substantial differences in the quantum yields occurred in the bound forms of ODN1Ap3, ODN1Ap9, and ODN2Ap5, though in all these sequences 2Ap is surrounded by a TG motif and a C residue. This suggests that NC does not bind similarly to the TGApC motifs in these ODNs. Fluorescence lifetime experiments (Table 1 of the Supporting Information) further revealed that as previously reported with hexanucleotides (*41*), NC restricts the collisions of 2Ap with its neighbor bases and strongly decreases the population of the fully stacked conformations of the probe.

Site-Specific Determination of NC−Dodecanucleotide Binding Parameters. (i) Binding Stoichiometry. To determine the stoichiometry of the NC−ODN complexes, time-resolved anisotropy decay experiments were performed to characterize the different rotational motions of the labeled species. The rotational correlation time associated with the tumbling of the labeled species is of special interest, since it depends on the hydrodynamic radius and, thus, on the molecular mass of the labeled species (*48*). In most free ODNs, the quantum yield of 2Ap was too low to obtain reliable time-resolved anisotropy parameters. In contrast, the higher quantum yields of the NC−ODN complexes allowed us to analyze their anisotropy decay curves. Three rotational correlation times were needed for good fitting of the anisotropy decay curves (Table 2), in contrast to the NC−hexanucleotide complexes which needed two components only (*41*). This increased complexity is probably associated with a more complicated set of local motions in the longer sequences. The two shorter components (~0.1−0.2 and 1−1.5 ns, respectively) presumably correspond to local rotations of the dye and/or segments of the ODNs, while the longest component (φ_3) is attributed to the tumbling of the whole complex. φ_3 values ranged from 7.5 to 10.7 ns. These values are significantly higher than the theoretical correlation time of 4.7 ns calculated for the tumbling of a sphere with the molecular mass of a 1:1 NC−ODN complex but are consistent with the theoretical correlation time of 7.5 ns calculated for a 2:1 NC−ODN complex. Deviations of the measured φ_3 values from this last value are likely due to the nonspherical shape of the complexes, as observed previously with the 1:1 complexes of NC with hexanucleotides (*41*). Thus, all tested ODNs were able to bind two NC molecules. To confirm the stoichiometry of the complexes, time-resolved anisotropy experiments were repeated using the same ODNs labeled at their 5′-terminus with Alexa430, a highly fluorescent dye. For the free ODNs, two rotational correlation times were determined (Table 3). The faster component (φ_1 = 0.2 ns) describes the local rotation of the dye. The slower component (1.1−1.4 ns) is somewhat below the theoretical rotational correlation time (1.8 ns) of a sphere with the molecular mass of the free ODNs, indicating that both tumbling and segmental motions of the ODNs likely contribute to this rotational correlation time (*49*). Both the large amplitude associated with the local motion and the contributions of segmental motions to the slower component are fully consistent with the high flexibility of the free ODNs, which allows conformational fluctuations in the picosecond to nanosecond time range. Binding of NC was found to strongly modify the time-resolved anisotropy decays of the Alexa430-labeled ODNs. As for the complexes with the 2Ap-labeled ODNs, three rotational correlation times were needed to describe the anisotropy decays of the complexes with Alexa430-labeled ODNs. The values of the slow rotational correlation time (φ_3 = 7.3−8.8 ns) were fully consistent with the values of the corresponding components

Table 2: Time-Resolved Anisotropy Parameters for the 2Ap-Substituted Dodecanucleotides Bound to NCp7[a]

	sequence	φ_1 (ns)	β_1	φ_2 (ns)	β_2	φ_3 (ns)	β_3
	free 2Ap	0.08	1.00				
ODN1Ap3	TG**Ap**CCGTGACCG	0.32	0.23	1.1	0.22	9.6	0.55
ODN1Ap9	TGACCGTG**Ap**CCG	0.12	0.21	1.0	0.25	7.5	0.54
ODN2Ap2	A**Ap**TGACTGAAAC	0.15	0.40	1.6	0.13	8.8	0.47
ODN2Ap5	AATG**Ap**CTGAAAC	0.10	0.29	1.3	0.15	8.5	0.56
ODN2Ap10	AATGACTGA**Ap**AC	0.23	0.52	1.6	0.12	9.3	0.36
ODN3Ap3	AA**Ap**CTGAATGAC	0.13	0.14	0.9	0.29	8.4	0.57
ODN3Ap7	AAACTG**Ap**ATGAC	0.30	0.34	1.3	0.12	9.5	0.54
ODN3Ap11	AAACTGAATG**Ap**C	0.11	0.39	1.4	0.31	11	0.30

[a] The fluorescence rotational correlation times (φ_i) and their amplitudes (β_i) were obtained from the time-resolved anisotropy decays, as described in Materials and Methods. Standard deviations for the rotational correlation times and amplitudes are less than 20 and 15%, respectively. Experiments were performed with 0.5−1.0 μM ODNs and 7.5 μM NC in 0.05 M HEPES (pH 7.5) in the absence of NaCl. Taking into account the affinities at 0.1 M NaCl (Table 1) and the salt dependence of NC binding to ODNs (*23, 40*), all binding sites are likely saturated with NC under these conditions. The addition of a third rotational correlation time in the fit to the experimental decay of the NC−ODN complexes decreased the χ^2 values from 2 to 1.1−1.3.

Table 3: Time-Resolved Anisotropy Parameters of Alexa430-Labeled Dodecanucleotides and Their Complexes with NC[a]

	sequence	NC	φ_1 (ns)	β_1	φ_2 (ns)	β_2	φ_3 (ns)	β_3
Alexa430−ODN1	TGACCGTGACCG	−	0.22	0.58	1.4	0.42		
		+	0.47	0.39	3.5	0.18	7.3	0.43
ODN1−Alexa430	TGACCGTGACCG	−	0.25	0.50	1.4	0.50		
		+	0.19	0.36	1.5	0.30	7.9	0.34
Alexa430−ODN2	AATGACTGAAAC	−	0.22	0.63	1.4	0.37		
		+	0.39	0.34	1.7	0.21	7.5	0.45
Alexa430−ODN3	AAACTGAATGAC	−	0.21	0.61	1.3	0.39		
		+	0.34	0.25	1.4	0.35	8.8	0.40
Alexa430−ODN4	TGACCGAAACAA	+	0.09	0.06	0.7	0.29	6.1	0.65
Alexa430−ODN5	AATGACCGAAAC	+	0.14	0.30	1.0	0.30	5.9	0.40

[a] Parameter significance and standard deviations are as in Table 2. Experiments were performed with 0.2 μM ODN in the absence or presence of 2 μM NC.

in the complexes with the 2Ap-labeled sequences, confirming the 2:1 stoichiometry of the NC−ODN complexes. Moreover, the large amplitude associated with this slow component as well as the absence of any contribution from segmental motions in this component confirmed that NC reduces the flexibility of the ODN and, thus, restricts its picosecond to nanosecond conformational fluctuations. Alexa430 attached to the 3′-terminus yielded the same results (Table 3), suggesting that the position of the dye does not affect the shape and the size of the complexes.

Thus, anisotropy decay data with Alexa430- and 2Ap-labeled ODNs are consistent with a 2:1 stoichiometry for all NC−ODN complexes, as expected from the two high-affinity TG motifs in their sequences (*22, 23, 30*). To demonstrate the central role of the TG motifs in the binding of the two NC molecules, two mutated Alexa430-labeled ODNs were used. The AATGACCGAAAC sequence (ODN4) corresponds to the ODN1 sequence in which the 3′-terminal TGACCG sequence was substituted with the poorly binding AAACAA sequence (*23*). The ODN5 sequence (AATGAC-CGAAAC) corresponded to the ODN2 sequence with a single $T^7 \rightarrow C$ mutation that substitutes the central TG motif with a lower-affinity CG motif. With both ODN4 and ODN5 sequences, the slow rotational correlation time dropped to a value of ~6 ns, between the theoretical correlation times of 4.7 and 7.5 ns for spheres with the molecular masses of the 1:1 and 2:1 NC−ODN complexes, respectively. Thus, the more likely explanation is that the complexes of NC with these two ODNs are nonspherical 1:1 complexes, confirming the central role of the TG motifs in the binding sites of the ODN1−ODN3 sequences for the NC molecules.

(ii) Binding Constants. As a consequence of the two TG binding sites in the ODN1, ODN2, and ODN3 sequences, a binding scheme with two individual binding sites was used to model the interaction of NC with these sequences:

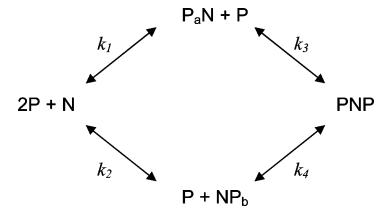

where P is the free protein, N is the free oligonucleotide, P_aN and NP_b are the 1:1 protein−ODN complexes with the protein bound to the proximal (5′-terminal) and distal (3′-terminal) binding sites, respectively (termed "a" and "b" sites, respectively), PNP is the 2:1 protein−ODN complex, and k_1-k_4 are the microscopic equilibrium binding constants. Since 2Ap fluorescence within ODNs is sensitive to changes in its immediate vicinity (*41, 46, 50, 51*), 2Ap should report on NC binding only to the site in which it is included. Using these assumptions, titrations of the various 2Ap-labeled ODNs with NC were used to calculate the concentrations of NC bound to the 2Ap-labeled binding site from the relative increase in 2Ap fluorescence. For instance, for a given ODN labeled at binding site a, the concentration of bound protein at this site is given by

$$\frac{PN_a + PNP}{N_t} = \frac{I_a - I_{a0}}{I_{af} - I_{a0}}$$

where I_a is the 2Ap fluorescence intensity at a given total protein concentration (P_t), I_{a0} and I_{af} are the 2Ap fluorescence intensities in the absence and presence of saturating NC concentrations, respectively, and N_t is the total ODN concentration expressed in species. In contrast, the concentration of free NC, also necessary to draw the binding isotherm and to calculate the binding constants, cannot be determined from a single titration curve, since it also depends on the binding of NC to the nonlabeled binding site. To overcome this, we titrated in parallel equal concentrations of an ODN labeled with 2Ap at the proximal binding site (a) and the same ODN labeled at the distal site (b). Under these conditions, the concentration of free protein P can be calculated by

$$P = P_t - N_t\left(\frac{I_a - I_{a0}}{I_{af} - I_{a0}} + \frac{I_b - I_{b0}}{I_{bf} - I_{b0}}\right) \quad (3)$$

After determination of P values for the various couples of I_a and I_b values, the titration data were replotted as $(I - I_0)/(I_f - I_0)$ versus P (Figure 3) and the microscopic affinity constants for all binding sites were determined by fitting the data to the following equations:

$$\frac{I_a - I_{a0}}{I_{af} - I_{a0}} = \frac{k_1P + k_1k_3P^2}{1 + (k_1 + k_2)P + k_1k_3P^2} \quad (4a)$$

$$\frac{I_b - I_{b0}}{I_{bf} - I_{b0}} = \frac{k_2P + k_1k_3P^2}{1 + (k_1 + k_2)P + k_1k_3P^2} \quad (4b)$$

where k_1 and k_2 are the microscopic affinity constants for NC binding to sites a and b, respectively. For all sequences, we observed substantial 2Ap position-dependent differences between the titration curves (Figure 3), consistent with our hypothesis that 2Ap reports NC binding at a given site. For the ODN1 sequence, the curve for binding of NC to ODN1Ap9 was significantly shifted toward the low concentrations of the free peptide with respect to the titration curve of ODN1Ap3. The two titration curves were fitted simultaneously to eqs 4a and 4b. Good fits were obtained, assuming that the binding sites were independent, and thus that $k_3 = k_2$ and $k_4 = k_1$. The binding constants in Table 1 were in line with the previously reported binding constants for binding of NC for TG-containing hexanucleotides (*23, 41*). Moreover, these binding constants show that the b site binds NC with a 3.5-fold higher affinity than the a site even though the ODN1 sequence is a repeat of two TGACCG motifs. This indicates that NC binding to the two TGACCG motifs is context-dependent.

With the ODN2 sequence, the binding curves of ODN2Ap2 and ODN2Ap5 sequences were superimposable (Figure 3B) and clearly shifted to high P concentrations, with respect to the ODN2Ap10 titration curve. This suggests that 2Ap at positions 2 and 5 sensed the binding of NC to the same binding site and that this site had a weaker affinity than the one containing the 2Ap residue at position 10. The fact that the nucleotides at positions 2 and 5 were constitutive of a unique binding site was not surprising since these two residues flanked the central ^{3}TG^4 motif critical for NC binding. In contrast, 2Ap at position 10 is likely associated with the ^{7}TG^8-containing distal site of the ODN. As in the case of ODN1, a good fit of the two titration curves was obtained, assuming that the binding sites were independent. The binding constants of the two sites differed by a factor of 2.

For ODN3, analysis of the ODN3Ap3 and ODN3Ap11 binding curves (Figure 3C) revealed that the affinity ($k_1 = 6.6 \times 10^5$ M^{-1}) of the proximal binding site with the ^{5}TG^6 motif was 50% higher than the affinity ($k_2 = 4.4 \times 10^5$ M^{-1}) of the distal binding site with the ^{9}TG^{10} motif. Surprisingly, the binding curve of ODN3Ap7 matched with neither of the two preceding curves and was clearly shifted to lower P concentrations, suggesting a higher affinity. Using eq 4a or 4b, an apparent binding constant of 1.1×10^6 M^{-1}, corresponding to the sum of k_1 and k_2, was obtained. Though 2Ap at position 7 flanks the G^6 residue of the proximal binding site, it is likely sensitive to the binding to both sites, due to its spatial proximity to the distal site. To check this hypothesis, we derived an equation in which we assume that the binding of NC to either site provides the same increase in 2Ap fluorescence and that no further increase occurs when both sites are bound:

$$\frac{I - I_0}{I_f - I_0} = \frac{I_a - I_{a0}}{I_{af} - I_{a0}} + \frac{I_b - I_{b0}}{I_{bf} - I_{b0}} = \frac{(k_1 + k_2)P + k_1k_3P^2}{1 + (k_1 + k_2)P + k_1k_3P^2} \quad (5)$$

The fit of the ODN3Ap7 binding curve with eq 5 provided k_1 and k_2 values (Table 1) that were in excellent agreement with the values obtained from the fits of the ODN3Ap3 and ODN3Ap11 binding curves, confirming our hypothesis. Thus, the labeling position should be carefully selected to site-selectively monitor the binding of NC.

DISCUSSION

Here we report the first site-specific characterization of NC binding to ODNs with multiple binding sites. An environment-sensitive fluorescent base analogue 2Ap was used for this purpose. In all sequences, 2Ap substituted adenine, which minimally perturbs the ODN properties (Figure 2).

In line with the literature (*47, 49*−*51*) and our recent study (*41*), we observed a strong quenching of 2Ap within the dodecanucleotides, which was dependent on the nature of the flanking bases, the strongest quenching being obtained with G. Interestingly, the quantum yield of 2Ap flanked by a G increases when 2Ap is near the ODN termini. This is likely a consequence of the higher flexibility of the ODN termini, which leads to a less efficient staking of the bases. As previously shown with hexanucleotides (*41*), a strong increase in the 2Ap quantum yield (Table 1) occurred upon NC binding. This increase was most pronounced (up to 15-fold) for sequences where 2Ap was flanked by G and was attributed both to NC-induced constraints on ODN flexibility and to specific interactions of NC with the bases flanking the fluorophore, such as the stacking of the Trp37 residue with the flanking guanine (*41*). Smaller fluorescence increases (<3-fold) were observed when 2Ap was more distant from a TG motif (AA**Ap**CTGAATGAC and AATGACTGAA**Ap**AC), in line with the preferential binding of NC to TG motifs (*22, 23*). Noticeably, NC does not always induce

a 2Ap fluorescence increase on interaction with ODNs, since a 10% fluorescence decrease was reported to accompany NC binding to a bulged 2Ap residue in a stem−loop motif (*52*). In this case, the 2Ap residue was only poorly stacking with its neighbors in the free ODN, as suggested by its high fluorescence intensity. As a consequence, the NC-induced changes in the ODN flexibility and the local mobility of the bases (including 2Ap) could only marginally affect the stacking and, thus, the fluorescence intensity of this bulged 2Ap.

All studied dodecanucleotides were found to bind two NC molecules at physiological salt concentrations, confirming the preferential binding of NC to the TG motifs and an occluded binding site size of five to six bases (*22, 23, 30, 53*). Importantly, strong similarities in the binding curves were observed when 2Ap residues were at close positions in a given ODN (for instance, at positions 2 and 5 in ODN2). In contrast, significant shifts in the binding curves occurred when 2Ap residues were distant (for instance, at positions 2 and 9 in ODN2). This clearly suggests that 2Ap at a given position responds mainly to the binding of NC to its closest TG motif, enabling site-specific investigations of NC binding to ODNs with multiple binding sites. Using two parallel titrations of the same ODN labeled with 2Ap at distant positions and assuming independent binding sites, we obtained the microscopic binding constants of the two TG-containing binding motifs. To the best of our knowledge, this constitutes the first direct characterization of two NC binding sites on the same ODN. This approach appears to be an interesting alternative to NMR titrations that require much higher ODN concentrations and thus can only be used for systems with rather low affinities. However, proper selection of the labeled position is critical in the proposed methodology since in the case of ODN3, the 2Ap label at position 7, between the two close TG motifs, was found to be sensitive to the binding of NC to both sites.

Using this approach based on 2Ap labeling at different positions, we found that the affinities of the TG-containing motifs range from 0.4×10^6 to 1.8×10^6 M^{-1}, suggesting that the binding of NC to these motifs is context-dependent. In this respect, ODN1 composed of two TGACCG motifs is of special interest. We were expecting the same microscopic affinities for the two binding sites. In addition, the lifetime distributions for 2Ap at positions 3 and 9 were very similar, being consistent with the same local microenvironment. However, the affinity constant for the proximal binding site is substantially lower than that for the distal binding site. This difference may be explained by the involvement of two guanines (G^6 and G^8) in NC binding to the distal binding site. Indeed, two alternative modes of NC binding to target ODNs are known from NMR structures. The first one, found for d(ACGCC) or (−)PBS, involves the interaction of both zinc fingers (F1 and F2) with a single G residue and its upstream base (*28, 30*). In the second mode found for SL3 (*29*), SL2 (*32*), or an U5 ODN from the 5′-untranslated region of HIV-1 (*31*), F1 and F2 interact through stacking of their aromatic amino acid (Phe16 in F1 and Trp37 in F2) with the two guanines of a GXG motif. This last type of binding is possible only for the distal motif of ODN1 where the G^6 and G^8 residues are properly spaced to allow their interaction with the two NC fingers. In contrast, only one guanine (G^2) is available for the binding of NC to the proximal binding site, which may explain its lower affinity, in line with the 1−2 order of magnitude lower affinities of NC for AATGCC (*23, 41*), the TG-containing loop of (−)PBS (*28, 37*), or SL3 and U5 mutants, where one G of the GXG motif has been substituted (*26, 31*) as compared to the affinity of NC for TGTGCC, $(TG)_4$, or the GXG binding motif of the U5 sequence and the SL2 and SL3 loops (*23, 27, 31, 32, 35*). In addition, the stability of the complex of NC with the proximal binding site of ODN1 may be further limited by the 5′-position of the TG motif.

For ODN2 and ODN3, the differences between the binding affinities of the proximal and distal binding sites were less pronounced, which does not allow us to draw clear conclusions. A larger set of ODNs with systematically varied bases would be needed to gain further information about the molecular determinants that modulate the affinity of NC for the individual binding sites. Nevertheless, since the affinities of the two sites differ by a factor of less than 4 in all three ODNs and were close to the affinities of the corresponding hexanucleotides, this excludes strong positive or negative cooperativity for the binding of NC to these dodecanucleotides. Such a limited cooperativity was already reported for the binding of NC to $(TG)_4$ (*35*), as well as to longer sequences, such as polyA (*38*), $tRNA^{Lys,3}$ (*39*), or (−)PBS (*28*). Since the TG binding motifs in ODN2 and ODN3 are separated by only two bases, the two bound NC molecules are necessarily very close, like on the short $(TG)_4$ sequence. In this respect, the weakly cooperative binding of NC suggests that no strong attraction or repulsion occurs between the bound NC molecules. Both the absence of strong negative cooperativity and the possibility of NC binding at very close binding sites are fully consistent with the extensive coating of the genomic RNA and the proviral DNA by NC to protect them against nucleases (*54*−*57*). In addition, the absence of strong positive cooperativity is in line with the required ability of NC to rapidly dissociate from the nucleic acids to exert its chaperone properties (*58*). Another consequence of our data is that ODNs able to bind several NC molecules with high affinity could be envisioned as therapeutic tools for dissociating the NC molecules bound to the HIV-1 genomic RNA and proviral DNA. Due to the critical role of NC in the HIV-1 life cycle, this dissociation should lead to a strong decrease in HIV-1 infectivity.

In conclusion, NC binding to the individual binding sites of dodecanucleotides was site-specifically characterized by using 2Ap fluorescence. This approach allowed us to determine the NC-induced changes in the local and overall ODN dynamics on the picosecond to nanosecond time scale. Furthermore, it allowed us to determine the microscopic binding constants of the individual binding sites. This last point constitutes a substantial advantage of this 2Ap-based approach over other commonly used techniques such as surface plasmon resonance, fluorescence anisotropy, isothermal titration calorimetry, mass spectroscopy, and ELISA, which do not respond site-specifically. This approach may be further extended to investigate the binding of NC (or any nucleic acid binding protein) to ODNs containing more than two binding sites, provided that the latter are not overlapping.

ACKNOWLEDGMENT

We thank H. de Rocquigny for peptide synthesis and G. Krishnamoorthy for providing the software for analysis of time-resolved fluorescence and anisotropy decay data.

SUPPORTING INFORMATION AVAILABLE

Fluorescence lifetime experiments with 2Ap-labeled ODNs and time-resolved intensity parameters for the 2Ap-substituted dodecanucleotides (Table 1). This material is available free of charge via the Internet at http://pubs.acs.org.

REFERENCES

1. Darlix, J. L., Cristofari, G., Rau, M., Pechoux, C., Berthoux, L., and Roques, B. (2000) Nucleocapsid protein of human immunodeficiency virus as a model protein with chaperoning functions and as a target for antiviral drugs. *Adv. Pharmacol. 48*, 345–372.
2. Clever, J., Sassetti, C., and Parslow, T. G. (1995) RNA secondary structure and binding sites for gag gene products in the 5′ packaging signal of human immunodeficiency virus type 1. *J. Virol. 69*, 2101–2109.
3. Bampi, C., Jacquenet, S., Lener, D., Decimo, D., and Darlix, J. L. (2004) The chaperoning and assistance roles of the HIV-1 nucleocapsid protein in proviral DNA synthesis and maintenance. *Int. J. Biochem. Cell Biol. 36*, 1668–1686.
4. Levin, J. G., Guo, J., Rouzina, I., and Musier-Forsyth, K. (2005) Nucleic acid chaperone activity of HIV-1 nucleocapsid protein: Critical role in reverse transcription and molecular mechanism. *Prog. Nucleic Acid Res. Mol. Biol. 80*, 217–286.
5. Rein, A., Henderson, L. E., and Levin, J. G. (1998) Nucleic-acid-chaperone activity of retroviral nucleocapsid proteins: Significance for viral replication. *Trends Biochem. Sci. 23*, 297–301.
6. D'Souza, V., and Summers, M. F. (2005) How retroviruses select their genomes. *Nat. Rev. Microbiol. 3*, 643–655.
7. Mely, Y., De Rocquigny, H., Morellet, N., Roques, B. P., and Gerard, D. (1996) Zinc binding to the HIV-1 nucleocapsid protein: A thermodynamic investigation by fluorescence spectroscopy. *Biochemistry 35*, 5175–5182.
8. Mely, Y., Jullian, N., Morellet, N., De Rocquigny, H., Dong, C. Z., Piemont, E., Roques, B. P., and Gerard, D. (1994) Spatial proximity of the HIV-1 nucleocapsid protein zinc fingers investigated by time-resolved fluorescence and fluorescence resonance energy transfer. *Biochemistry 33*, 12085–12091.
9. Morellet, N., Jullian, N., De Rocquigny, H., Maigret, B., Darlix, J. L., and Roques, B. P. (1992) Determination of the structure of the nucleocapsid protein NCp7 from the human immunodeficiency virus type 1 by 1H NMR. *EMBO J. 11*, 3059–3065.
10. Summers, M. F., Henderson, L. E., Chance, M. R., Bess, J. W., Jr., South, T. L., Blake, P. R., Sagi, I., Perez-Alvarado, G., Sowder, R. C., and Hare, D. R. (1992) Nucleocapsid zinc fingers detected in retroviruses: EXAFS studies of intact viruses and the solution-state structure of the nucleocapsid protein from HIV-1. *Protein Sci. 1*, 563–574.
11. Aldovini, A., and Young, R. A. (1990) Mutations of RNA and protein sequences involved in human immunodeficiency virus type 1 packaging result in production of noninfectious virus. *J. Virol. 64*, 1920–1926.
12. Demene, H., Dong, C. Z., Ottmann, M., Rouyez, M. C., Jullian, N., Morellet, N., Mely, Y., Darlix, J. L., Fournie-Zaluski, M. C., Saragosti, S., et al. (1994) ^{1}H NMR structure and biological studies of the His23 → Cys mutant nucleocapsid protein of HIV-1 indicate that the conformation of the first zinc finger is critical for virus infectivity. *Biochemistry 33*, 11707–11716.
13. Dorfman, T., Luban, J., Goff, S. P., Haseltine, W. A., and Gottlinger, H. G. (1993) Mapping of functionally important residues of a cysteine-histidine box in the human immunodeficiency virus type 1 nucleocapsid protein. *J. Virol. 67*, 6159–6169.
14. Gorelick, R. J., Gagliardi, T. D., Bosche, W. J., Wiltrout, T. A., Coren, L. V., Chabot, D. J., Lifson, J. D., Henderson, L. E., and Arthur, L. O. (1999) Strict conservation of the retroviral nucleocapsid protein zinc finger is strongly influenced by its role in viral infection processes: characterization of HIV-1 particles containing mutant nucleocapsid zinc-coordinating sequences. *Virology 256*, 92–104.
15. Gorelick, R. J., Nigida, S. M., Jr., Bess, J. W., Jr., Arthur, L. O., Henderson, L. E., and Rein, A. (1990) Noninfectious human immunodeficiency virus type 1 mutants deficient in genomic RNA. *J. Virol. 64*, 3207–3211.
16. Guo, J., Wu, T., Anderson, J., Kane, B. F., Johnson, D. G., Gorelick, R. J., Henderson, L. E., and Levin, J. G. (2000) Zinc finger structures in the human immunodeficiency virus type 1 nucleocapsid protein facilitate efficient minus- and plus-strand transfer. *J. Virol. 74*, 8980–8988.
17. Ottmann, M., Gabus, C., and Darlix, J. L. (1995) The central globular domain of the nucleocapsid protein of human immunodeficiency virus type 1 is critical for virion structure and infectivity. *J. Virol. 69*, 1778–1784.
18. Ramboarina, S., Morellet, N., Fournie-Zaluski, M. C., and Roques, B. P. (1999) Structural investigation on the requirement of CCHH zinc finger type in nucleocapsid protein of human immunodeficiency virus 1. *Biochemistry 38*, 9600–9607.
19. Stote, R. H., Kellenberger, E., Muller, H., Bombarda, E., Roques, B. P., Kieffer, B., and Mely, Y. (2004) Structure of the His44 → Ala single point mutant of the distal finger motif of HIV-1 nucleocapsid protein: A combined NMR, molecular dynamics simulation, and fluorescence study. *Biochemistry 43*, 7687–7697.
20. Thomas, J. A., and Gorelick, R. J. (2008) Nucleocapsid protein function in early infection processes. *Virus Res. 134*, 39–63.
21. de Rocquigny, H., Shvadchak, V., Avilov, S., Dong, C. Z., Dietrich, U., Darlix, J. L., and Mely, Y. (2008) Targeting the viral nucleocapsid protein in anti-HIV-1 therapy. *Mini-Rev. Med. Chem. 8*, 24–35.
22. Fisher, R. J., Rein, A., Fivash, M., Urbaneja, M. A., Casas-Finet, J. R., Medaglia, M., and Henderson, L. E. (1998) Sequence-specific binding of human immunodeficiency virus type 1 nucleocapsid protein to short oligonucleotides. *J. Virol. 72*, 1902–1909.
23. Vuilleumier, C., Bombarda, E., Morellet, N., Gerard, D., Roques, B. P., and Mely, Y. (1999) Nucleic acid sequence discrimination by the HIV-1 nucleocapsid protein NCp7: A fluorescence study. *Biochemistry 38*, 16816–16825.
24. You, J. C., and McHenry, C. S. (1993) HIV nucleocapsid protein. Expression in *Escherichia coli*, purification, and characterization. *J. Biol. Chem. 268*, 16519–16527.
25. Hagan, N., and Fabris, D. (2003) Direct mass spectrometric determination of the stoichiometry and binding affinity of the complexes between nucleocapsid protein and RNA stem-loop hairpins of the HIV-1 Psi-recognition element. *Biochemistry 42*, 10736–10745.
26. Paoletti, A. C., Shubsda, M. F., Hudson, B. S., and Borer, P. N. (2002) Affinities of the nucleocapsid protein for variants of SL3 RNA in HIV-1. *Biochemistry 41*, 15423–15428.
27. Shubsda, M. F., Paoletti, A. C., Hudson, B. S., and Borer, P. N. (2002) Affinities of packaging domain loops in HIV-1 RNA for the nucleocapsid protein. *Biochemistry 41*, 5276–5282.
28. Bourbigot, S., Ramalanjaona, N., Boudier, C., Salgado, G. F., Roques, B. P., Mely, Y., Bouaziz, S., and Morellet, N. (2008) How the HIV-1 Nucleocapsid Protein Binds and Destabilises the (−)Primer Binding Site During Reverse Transcription. *J. Mol. Biol. 383*, 1112–1128.
29. De Guzman, R. N., Wu, Z. R., Stalling, C. C., Pappalardo, L., Borer, P. N., and Summers, M. F. (1998) Structure of the HIV-1 nucleocapsid protein bound to the SL3 psi-RNA recognition element. *Science 279*, 384–388.
30. Morellet, N., Demene, H., Teilleux, V., Huynh-Dinh, T., de Rocquigny, H., Fournie-Zaluski, M. C., and Roques, B. P. (1998) Structure of the complex between the HIV-1 nucleocapsid protein NCp7 and the single-stranded pentanucleotide d(ACGCC). *J. Mol. Biol. 283*, 419–434.
31. Spriggs, S., Garyu, L., Connor, R., and Summers, M. F. (2008) Potential Intra- and Intermolecular Interactions Involving the Unique-5′ Region of the HIV-1 5′-UTR. *Biochemistry 47*, 13064–13073.
32. Amarasinghe, G. K., De Guzman, R. N., Turner, R. B., Chancellor, K. J., Wu, Z. R., and Summers, M. F. (2000) NMR structure of the HIV-1 nucleocapsid protein bound to stem-loop SL2 of the psi-RNA packaging signal. Implications for genome recognition. *J. Mol. Biol. 301*, 491–511.
33. Beltz, H., Clauss, C., Piemont, E., Ficheux, D., Gorelick, R. J., Roques, B., Gabus, C., Darlix, J. L., de Rocquigny, H., and Mely, Y. (2005) Structural determinants of HIV-1 nucleocapsid protein for cTAR DNA binding and destabilization, and correlation with inhibition of self-primed DNA synthesis. *J. Mol. Biol. 348*, 1113–1126.

34. Egele, C., Piemont, E., Didier, P., Ficheux, D., Roques, B., Darlix, J. L., de Rocquigny, H., and Mely, Y. (2007) The single-finger nucleocapsid protein of moloney murine leukemia virus binds and destabilizes the TAR sequences of HIV-1 but does not promote efficiently their annealing. *Biochemistry 46*, 14650–14662.
35. Fisher, R. J., Fivash, M. J., Stephen, A. G., Hagan, N. A., Shenoy, S. R., Medaglia, M. V., Smith, L. R., Worthy, K. M., Simpson, J. T., Shoemaker, R., McNitt, K. L., Johnson, D. G., Hixson, C. V., Gorelick, R. J., Fabris, D., Henderson, L. E., and Rein, A. (2006) Complex interactions of HIV-1 nucleocapsid protein with oligonucleotides. *Nucleic Acids Res. 34*, 472–484.
36. Beltz, H., Piemont, E., Schaub, E., Ficheux, D., Roques, B., Darlix, J. L., and Mely, Y. (2004) Role of the structure of the top half of HIV-1 cTAR DNA on the nucleic acid destabilizing activity of the nucleocapsid protein NCp7. *J. Mol. Biol. 338*, 711–723.
37. Egele, C., Schaub, E., Ramalanjaona, N., Piemont, E., Ficheux, D., Roques, B., Darlix, J. L., and Mely, Y. (2004) HIV-1 nucleocapsid protein binds to the viral DNA initiation sequences and chaperones their kissing interactions. *J. Mol. Biol. 342*, 453–466.
38. Khan, R., and Giedroc, D. P. (1994) Nucleic acid binding properties of recombinant Zn2 HIV-1 nucleocapsid protein are modulated by COOH-terminal processing. *J. Biol. Chem. 269*, 22538–22546.
39. Mely, Y., de Rocquigny, H., Sorinas-Jimeno, M., Keith, G., Roques, B. P., Marquet, R., and Gerard, D. (1995) Binding of the HIV-1 nucleocapsid protein to the primer tRNA(3Lys), in vitro, is essentially not specific. *J. Biol. Chem. 270*, 1650–1656.
40. Urbaneja, M. A., Kane, B. P., Johnson, D. G., Gorelick, R. J., Henderson, L. E., and Casas-Finet, J. R. (1999) Binding properties of the human immunodeficiency virus type 1 nucleocapsid protein p7 to a model RNA: Elucidation of the structural determinants for function. *J. Mol. Biol. 287*, 59–75.
41. Avilov, S. V., Piemont, E., Shvadchak, V., de Rocquigny, H., and Mely, Y. (2008) Probing dynamics of HIV-1 nucleocapsid protein/target hexanucleotide complexes by 2-aminopurine. *Nucleic Acids Res. 36*, 885–896.
42. de Rocquigny, H., Ficheux, D., Gabus, C., Fournie-Zaluski, M. C., Darlix, J. L., and Roques, B. P. (1991) First large scale chemical synthesis of the 72 amino acid HIV-1 nucleocapsid protein NCp7 in an active form. *Biochem. Biophys. Res. Commun. 180*, 1010–1018.
43. Zuker, M. (2003) Mfold web server for nucleic acid folding and hybridization prediction. *Nucleic Acids Res. 31*, 3406–3415.
44. Ward, D. C., Reich, E., and Stryer, L. (1969) Fluorescence studies of nucleotides and polynucleotides. I. Formycin, 2-aminopurine riboside, 2,6-diaminopurine riboside, and their derivatives. *J. Biol. Chem. 244*, 1228–1237.
45. Ben Gaied, N., Glasser, N., Ramalanjaona, N., Beltz, H., Wolff, P., Marquet, R., Burger, A., and Mely, Y. (2005) 8-Vinyl-deoxyadenosine, an alternative fluorescent nucleoside analog to 2′-deoxyribosyl-2-aminopurine with improved properties. *Nucleic Acids Res. 33*, 1031–1039.
46. Nag, N., Ramreddy, T., Kombrabail, M., Krishna Mohan, P. M., D'Souza, J., Rao, B. J., Duportail, G., Mely, Y., and Krishnamoorthy, G. (2006) in *Reviews in Fluorescence* (Geddes, C., and Lakowicz, J. R., Eds.) pp 311−340, Springer Science, New York.
47. Guest, C. R., Hochstrasser, R. A., Sowers, L. C., and Millar, D. P. (1991) Dynamics of mismatched base pairs in DNA. *Biochemistry 30*, 3271–3279.
48. Lakowicz, J. R. (1999) *Principles of Fluorescence Spectroscopy*, 2nd ed., Kluwer Academic/Plenum Publishers, Dordrecht, The Netherlands.
49. Ramreddy, T., Rao, B. J., and Krishnamoorthy, G. (2007) Site-Specific Dynamics of Strands in ss- and dsDNA As Revealed by Time-Domain Fluorescence of 2-Aminopurine. *J. Phys. Chem. B 111*, 5757–5766.
50. Jean, J. M., and Hall, K. B. (2004) Stacking-unstacking dynamics of oligodeoxynucleotide trimers. *Biochemistry 43*, 10277–10284.
51. Larsen, O. F., van Stokkum, I. H., Gobets, B., van Grondelle, R., and van Amerongen, H. (2001) Probing the structure and dynamics of a DNA hairpin by ultrafast quenching and fluorescence depolarization. *Biophys. J. 81*, 1115–1126.
52. Rist, M. J., and Marino, J. P. (2002) Mechanism of nucleocapsid protein catalyzed structural isomerization of the dimerization initiation site of HIV-1. *Biochemistry 41*, 14762–14770.
53. Karpel, R. L., Henderson, L. E., and Oroszlan, S. (1987) Interactions of retroviral structural proteins with single-stranded nucleic acids. *J. Biol. Chem. 262*, 4961–4967.
54. Buckman, J. S., Bosche, W. J., and Gorelick, R. J. (2003) Human immunodeficiency virus type 1 nucleocapsid Zn^{2+} fingers are required for efficient reverse transcription, initial integration processes, and protection of newly synthesized viral DNA. *J. Virol. 77*, 1469–1480.
55. Gao, K., Gorelick, R. J., Johnson, D. G., and Bushman, F. (2003) Cofactors for human immunodeficiency virus type 1 cDNA integration in vitro. *J. Virol. 77*, 1598–1603.
56. Krishnamoorthy, G., Roques, B., Darlix, J. L., and Mely, Y. (2003) DNA condensation by the nucleocapsid protein of HIV-1: A mechanism ensuring DNA protection. *Nucleic Acids Res. 31*, 5425–5432.
57. Tanchou, V., Gabus, C., Rogemond, V., and Darlix, J. L. (1995) Formation of stable and functional HIV-1 nucleoprotein complexes in vitro. *J. Mol. Biol. 252*, 563–571.
58. Cruceanu, M., Gorelick, R. J., Musier-Forsyth, K., Rouzina, I., and Williams, M. C. (2006) Rapid kinetics of protein-nucleic acid interaction is a major component of HIV-1 nucleocapsid protein's nucleic acid chaperone function. *J. Mol. Biol. 363*, 867–877.
59. Xu, D., Evans, K. O., and Nordlund, T. M. (1994) Melting and premelting transitions of an oligomer measured by DNA base fluorescence and absorption. *Biochemistry 33*, 9592–9599.

BI8022366